Hindawi
Geofluids
Volume 2023, Article ID 7540561, 17 pages
https://doi.org/10.1155/2023/7540561

Research Article

Analysis of the Influence of Groundwater Level Fluctuation on Karst Soil Cave Collapse

Xuejun Chen,[1,2] Mingming Xue,[1,2] and Yu Song[1,2]

[1]*College of Civil and Architecture Engineering, Guilin University of Technology, Guilin 541004, China*
[2]*Guangxi Key Laboratory of Geotechnical Mechanics and Engineering, Guilin University of Technology, Guilin 541004, China*

Correspondence should be addressed to Yu Song; songyu119@126.com

Received 22 July 2022; Revised 16 October 2022; Accepted 17 October 2022; Published 21 January 2023

Academic Editor: Yi Xue

Artificial water pumping and rainfall will induce groundwater level fluctuations, leading to large-scale karst collapse. Therefore, the combination of physical model test and FLAC3D numerical simulation is adopted to simulate the soil cave collapse caused by three different initial water level fluctuations in this paper. The influence of various initial water level heights on the variation of water-gas pressure, soil pressure of the overlying soil layer, and deformation in the existing soil cave during the fluctuation was analyzed. The relationship between initial water level height, deformation and collapse of the cave, and water-gas pressure was established, and the action law of water level fluctuations on the collapse of soil cave was introduced. The results show the following: (1) The change of water-gas pressure positively correlates with the initial water level height, directly affecting the overlying soil layer deformation. (2) The change of soil pressure of overlying soil positively correlates with the change of water-gas pressure under different initial water level fluctuations. (3) The deformation and collapse difficulty of the soil cave negatively correlates with the initial water level. The higher the initial water level, the stronger the negative pressure absorption and positive pressure gas explosion effect on the overburden on the soil cave and the collapse will occur with fewer water level fluctuations. (4) The numerical simulation results are consistent with the laboratory model test. These laws elucidate the change of water-gas pressure in different initial water level fluctuations and reveal the collapse mechanism of water level fluctuations. It will provide essential theoretical support for further research on the action law of hydrodynamic factors on karst collapse and a scientific and reasonable basis for urban groundwater pumping control, karst and roadbed collapse prevention and prediction.

1. Introduction

Hydrodynamic conditions, particularly groundwater-level change, are key factors leading to karst collapse. In recent years, the fluctuation of groundwater levels caused by artificial pumping and rainfall exacerbated subsurface erosion, negative pressure absorption, and positive pressure gas explosion [1–3]. It accelerated the collapse of karst soil caves, attracting researchers to study the collapse mechanism caused by groundwater fluctuations. Establishing mechanical and mathematical models can reveal the evolution of soil caves' underwater level change. Wang et al. improved the mechanical model of soil cave collapse based on the ultimate balance theory and accurately divided the evolution stages of soil caves [4–6]; Guo et al. established a ground subsidence mechanical model of covered karst soil caves considering the cave's shape and size under the condition of groundwater slump to reveal the internal relationship between the initial groundwater level, the shape and size of the cave, and the negative pressure of the soil cave cavity and clarified the influence of the negative pressure change caused by the water level drop on the stability of the soil cave evolution stage [7, 8]; Xue et al. conducted acoustic emission tests to measure the effect of CO_2 adsorption force on the mechanical properties of deep coal seams and established an elastic damage constitutive model of nonlinear stress-strain relationship and proposed the deformation and failure mechanism of deep coal seam due to the strength of gas adsorption force [9]. To the greatest extent, the field test can reflect the collapse process of karst soil caves under

hydrodynamic conditions [10]. Chen et al. carried out field pumping tests and clarified that the water level change caused by pumping is the main factor of collapse [11]; Jiang et al. and Jia et al. conducted long-term monitorization and analysis of the groundwater level change on site and revealed the formation mechanism of the soil cave collapse and the response of the deformation to the water level change [12, 13]. However, field test stress and boundary conditions are difficult to control and carry out. Many scholars study the effect of groundwater level changes on soil cave collapse by carrying out physical model tests [14–20]; Xiao et al. performed model tests to investigate the relationship between the relative strength degree and deformation of negative pressure suction and the effects of latent corrosion caused by water level changes. It reveals that the combined action of subsurface erosion and negative pressure absorption causes the mechanism of soil cave collapse [21, 22]; Zhang et al. and Hong et al. carried out water level fluctuation experiments to study the response of soil cave deformation to water level fluctuations and the characteristics of soil cave evolution at each stage [23, 24]. With the wide application of computers, numerical simulation was used to show the variation law of stress and displacement of the overlying soil during the change of water level [25–28]. Through numerical simulation showing the dynamic evolution process of soil caves under different water level drops, Xiong et al. determined the critical water level difference of collapse and provided a basis for karst prediction [29]. In addition, through the combination of mathematical mechanics model and model test, the law of water level change on soil cave collapse under the movement of various factors is comprehensively considered [30, 31].

Numerous researchers concluded the effect of water level changes on the impact of latent corrosion, negative pressure suction, and positive pressure gas explosion on soil caves from field and model tests. They expounded on the mechanical mechanism of soil cave collapse caused by water level change on numerical simulation, which is crucial theoretical support for studying hydrodynamic collapse. However, the current studies primarily employ a single model test or numerical simulation method, which cannot correspond well to the test results with the numerical simulation of stress and displacement distribution. Hence, it cannot comprehensively describe the effect of hydrodynamic conditions on soil cave collapse from the internal mechanical mechanism to the macroscopic phenomenon. In addition, most of the studies establish the relationship between hydrodynamic factors and soil cave collapse by controlling the rate and amplitude of water level change. However, there are deficiencies in the effect of different initial water level fluctuations on the collapse of karst soil caves and the dynamic response of water-gas pressure and further research is needed. Taking the karst collapse-prone areas in Lingui District, Guilin City as the research object, by collecting geological data, this paper constructs a generalized geological model to conduct physical model experiments and combined FLAC3D numerical simulation to simulate the evolution process of karst soil caves under different initial water level fluctuation conditions, while the water-gas pressure and temperatures in the existing soil cave and the deformation of the covering layer are monitored and compared with the numerical simulation results of stress, displacement, and plastic zone to propose a law to the effect of various initial water level fluctuations on soil cave collapse.

2. Environmental Geological Background of the Study Area

The studied area is located in Lingui District, Guilin City; it is at the southern end of the Xianggui Corridor with an average elevation of 150 meters above sea level from 109°36′ to 111°29′ east longitude and 24°15′ to 26°23′ north latitude. Meteorological survey shows that the total annual precipitation is 1266.0-1986.0 mm, the preflood season (April-June) is 627.0-1253.0 mm, and the postflood season (July-September) is 128.0-305.0 mm. Heavy rain mainly occurs from May to June with frequent anthropogenic water pumping and drastic changes in water level. The study area is a "∞" type karst basin with two basic structures: folds and faults, products of multistage tectonic movements, and most tectonic traces are NE and NW. The well-connected groundwater is classified into pore water and karst water; pore water is chiefly distributed in the gravel and silty clay layers in the alluvial-proluvial layer $Q_3^{al\text{-}pl}$ and the eluvial layer $Q_3^{dl\text{-}el}$. As shown in Figure 1, the studied area are mainly composed of the Upper Pleistocene alluvial-pluvial layer ($Q_3^{al\text{-}pl}$), the Upper Pleistocene eluvial layer ($Q_3^{dl\text{-}el}$), and the Upper Devonian Rongxian Formation (D_3r).

The lithological characteristics of each stratum are described as follows:

(1) Upper Pleistocene alluvial-pluvial layer ($Q_3^{al\text{-}pl}$): yellow, silty clay, composed of gravel, clay and a small amount of fine sand and pebbles, 2~14 m thick. The silty clay formed by the $Q_3^{al\text{-}pl}$ alluvial-proluvial layer has low clay content, correspondingly low consolidation degree and shear strength, and poor collapse resistance

(2) Upper Pleistocene eluvial layer ($Q_3^{dl\text{-}el}$): brick red, light yellow clay, sandy clay, containing a small number of quartz particles, 0.1~10 m thick

(3) Upper Devonian Rongxian Formation (D_3r): gray-white, slightly weathered, medium to thick layered, relatively complete rock mass. The main mineral is calcite, which is developed and tightly cemented. The karst fissures of bedrock surface are relatively developed

3. Geological Model Generalization and Test Scheme

3.1. Geological Model Generalization. Considering the complex geological conditions of the studied area, the generalization of the geological model is required. After collecting geological drilling data in Lingui District, Guilin City, it can be known that the overlying soil layer can be mainly

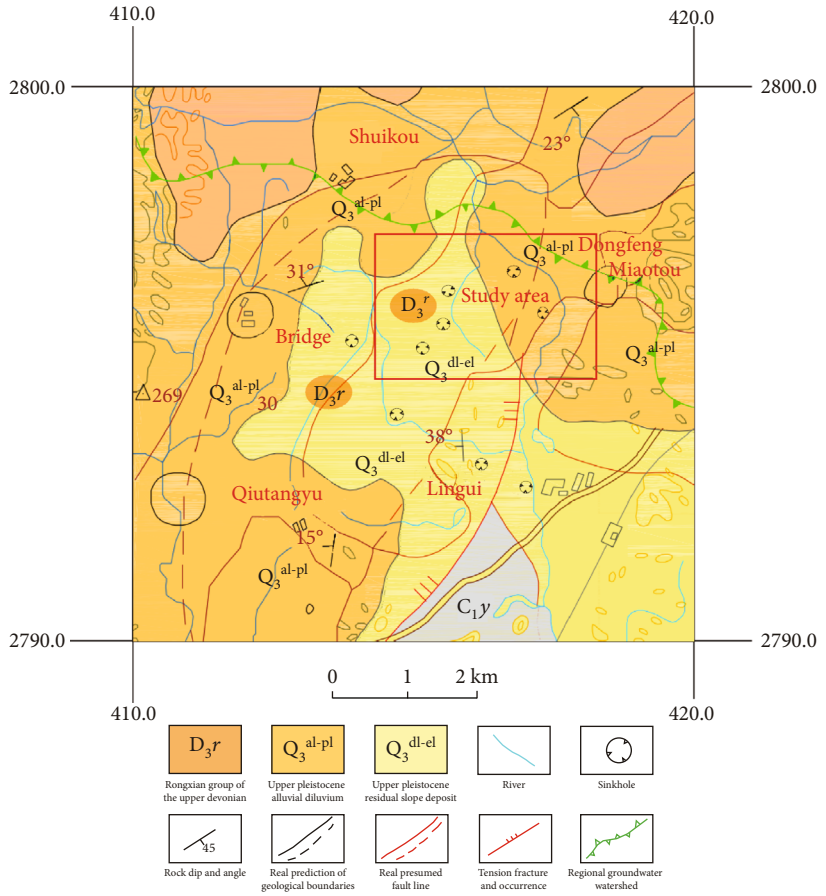

Figure 1: Engineering geological map.

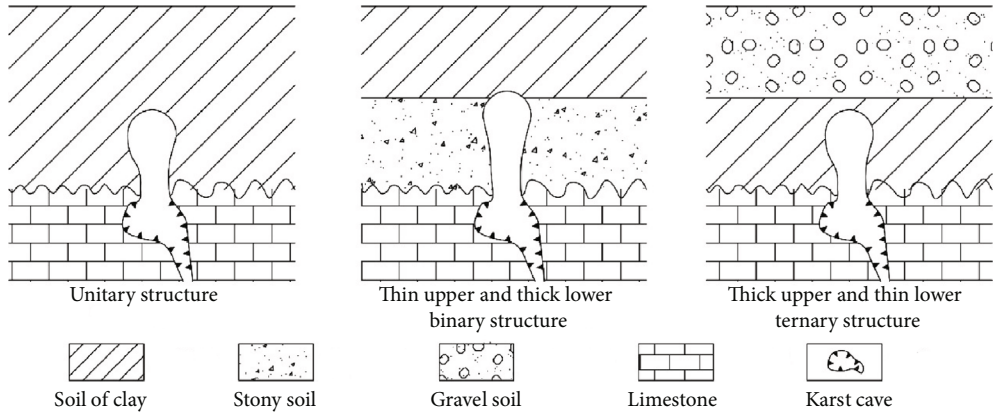

Figure 2: Structure types of overlying soil layers.

divided into the single-layer structure or double-layer structure (as shown in Figure 2).

In this paper, the single-layer structure (silty clay structure layer) is mainly used for simulation. The basic physical and mechanical property parameters of silty clay were measured by laboratory geotechnical tests (see Table 1 for details).

3.2. Physical Model Device Design. By investigating and collecting geological data in the study area and referring to the similarity theory [32] to determine the model similarity ratio as 1 : 10, a physical model device was independently designed (shown in Figure 3).

The frame of the device is made of hard aluminum alloy with high strength, and the side wall is inlaid with 5 mm

Table 1: Basic physical and mechanical parameters of soil.

Overlay type	Density (g/cm^3)	Porosity	Shear modulus (kPa)	Bulk modulus (kPa)	Internal friction angle (°)	Cohesion (kPa)	Permeability coefficient (cm/s)
Silty clay	1.72	0.47	1.354×10^6	4.22×10^6	8.8	25.3	3.22×10^{-4}

1-Sprinkler
2-The side sink
3-The surface of the scale
4-Soil cave
5-Water tank
6-Water tank inlet
7-Water tank drain
8-Tank drainage monitoring water meter
9-Video

(a)

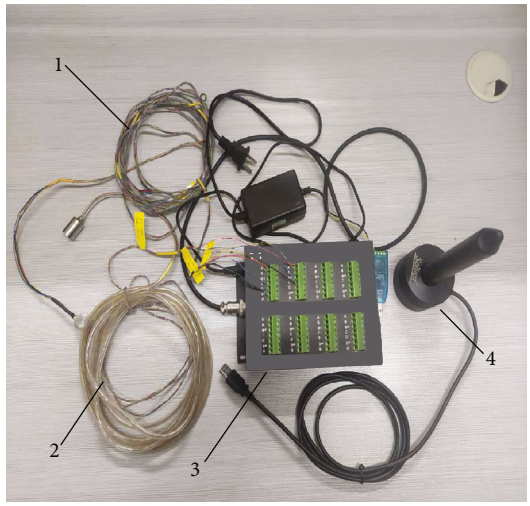

1-Soil pressure sensor
2-Pore-pressure sensor
3-Dynamic-static resistance deformeter
4-Automatic water level monitor

(b)

Figure 3: Physical model device and monitoring equipment.

thick tempered glass. The karst channel is set in a semicircle, and the karst channel mouth is set in a semicircle located at the front side's midpoint. There is a 1/4 sphere soil cave above the channel opening, and it is formed by preburied special ice cubes. The whole physical model test device consists of three parts: the main model, the water supply and drainage system, and the test system.

The size of the main model is 1200 mm in longitude, 700 mm in width, and 900 mm in height. The main model consists of upper and lower parts; the upper part is a soil box with a thickness of 600 mm, which is used to simulate the overlying soil layer; the lower part is a water tank with a height of 300 mm, which is used to simulate the karst cavity and water storage in the bedrock, and is connected to the upper soil box through a karst channel.

The soil box and the karst cavity have independent water supply and drainage systems, which can be adjusted according to the hydrodynamic conditions to reproduce the process of soil cave collapse at different initial water levels. The soil box's water supply and drainage system comprises the sink on the left and right sides and the drainage orifices on the bottom and side walls. When the water rises, the left and right sinks can control the water level in the upper soil layer to ensure a stable water head in the soil layer. When the water falls, water can be drained.

The water supply system of the karst cavity effectively supplies water to the water tank through the control switch of the external water pipe of the water tank. The water is stored in the tank, set to a closed state with a drainage orifice (diameter 100 mm) and a drain pipe on the side wall. When the drain pipe turns on, the water level drop (water pumping or groundwater runoff) in the karst cavity is simulated. The test system includes three functions: one is to record the water-air pressure and the temperature in the soil cavity in real-time through the Solinst water level automatic monitorization. The Solinst water level automatic monitor can reach an accuracy of ±0.05%, and the minimum sampling frequency is 0.125 s, which can realize high-frequency real-time data

Table 2: Model test scheme.

Scheme	Initial water level position	Initial water level height (mm)
1	Soil surface	100
2	Middle of the cave	25
3	Bedrock face	0

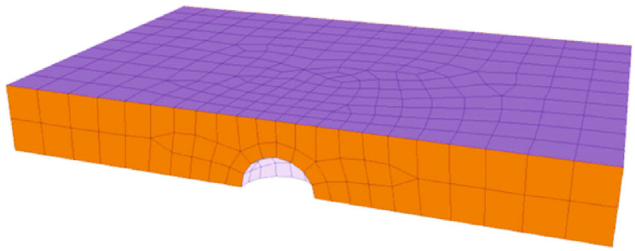

Figure 4: Karst model.

reading. In the test, the water level monitoring sensor was inserted into the fixed slot of the desktop reader connecting to the computer. The software was started to acquire data with the sampling frequency of every 1 s by setting water level, air pressure, temperature unit, and other parameters. The water level was automatically monitored when the water injection started. In this way, when the ice in the prefabricated soil cave melted, the water pressure and the temperatures in the soil cave during the rise and fall of water were monitored real-time.

The second is to monitor the overlying soil pressure through dynamic and static resistance strain instruments and soil pressure sensors. It adopts a 24-bit high-resolution conversion chip to realize the full-bridge measurement conversion of data, which connected the soil sensors to a short-circuited one. The soil pressure sensor was first connected to the resistance strain instruments in the test. The data transmission interface was connected to the computer to transmit the measured data to the computer-side data acquisition software employing electrical signals. The same interval between the water and air pressure acquisition data is stable and reliable. The soil pressure sensor measured the soil pressure within 30 kPa, with a maximum error within the rate of 0.5%, meeting the model test conditions. The force-bearing surface of the soil pressure sensor was placed in contact with the top of the soil cave (at a depth of 5 cm of the soil layer) and buried and compacted to fix it. Meanwhile, the other end connected the dynamic and static resistance strain instruments. The data acquisition can realize the real-time earth pressure monitoring of the overlying soil in the rise and fall of water.

The third is to record the whole process of deformation and damage of the overlying soil layer in the side wall in real-time through the camera.

3.3. Model Test and Numerical Simulation Scheme. The natural moisture content of the soil layer was tested to range from 19.1% to 22.6%, Combined with the actual properties of the soil and the average moisture content of soil layers at different depths measured by multiple pretests of 20%, the moisture content of the overlying soil in this model test was finally determined to be 20%. After multiple repeated vibration compmovement, the average compmovement dry density of the remodeled soil was determined to be 1.4 g/cm^3. The thickness of the overlying soil layer is 0.5~4.5 m, and the diameter of the bedrock surface opening is about 1 m. According to the geometrically similar proportion, the thickness of the silty clay covering layer in the simulation test was set to 10 cm, and the diameter of the soil cave was set to 10 cm, which is prefabricated and melted with ice cubes. We weigh the soil samples required for each experiment according to the size of the model device and the requirements of the experimental scheme and determine the stratification-thickness of the soil samples for each experiment and vibrate them with a small hand-held vibrator and load them into the model device in layers, and finally, the average compacted dry density of soil samples after filling is 1.4 g/cm^3, the average density is close to 85%, and the average moisture content is close to 20%.

Three initial water levels were set, taking the bedrock surface as the 0 reference level, which was located on the surface of the overburden, in the middle of the soil cave, and on the bedrock surface, which corresponded to the initial water level height of 100 mm, 25 mm, and 0 mm, respectively. Every time the water level falls, it went through a karst cavity from the initial water level and keep the same rates of water level rising and falling in the three experiments. The model test scheme is shown in Table 2.

The operation procedures of the three groups of experiments are the same. Taking the initial water level on the surface of the soil layer as an example, the experimental steps can be briefly described as follows:

(1) Turn on the water supply switch, adjust and control the rising speed of the water level through the valve of the water supply pipe until the initial water level just reaches the soil surface

(2) Turn off the water supply switch to make the water level drop from the soil surface to the karst cavity, which is a water level dropping process, and the water level dropping speed is adjusted and controlled by the drain valve

(3) After the water level drop process is over, repeat step (1) and (2) until the soil layer collapses. The water level should be ensured to rise and fall at the same speed each time

Numerical simulation adopts a 1 : 1 method with the physical model test. A karst model was established in the 3D modeling software (Rhino) (as shown in Figure 4), and the calculation grid was correctly divided and imported into FLAC3D, and the following steps were carried out:

(1) Establish three karst models with different initial water levels, assign the Mohr-Coulomb constitutive

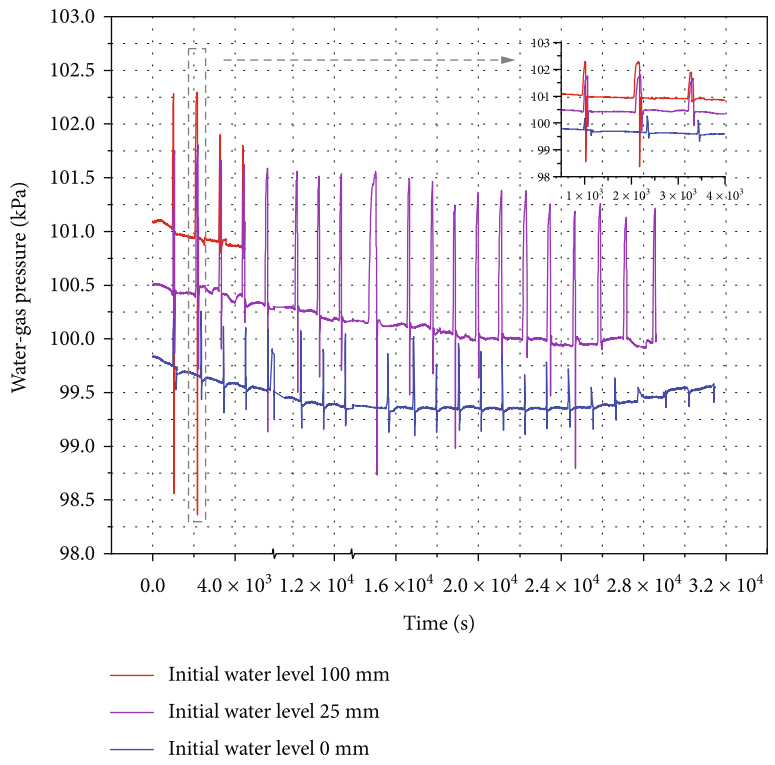

Figure 5: Variation of water-gas pressure with time.

Table 3: The amplitude of increase and decrease of water-gas pressure during the next water level rise and fall with different initial water level heights.

	Initial water level height (mm)				
Water level rises	100	Water-gas pressure increase amplitude (kPa)	1.26	1.364	1.003
	25		1.345	1.402	1.220
	0		0.441	0.616	0.529
Water level drops	100	Water-gas pressure drop amplitude (kPa)	3.723	3.932	1.101
	25		1.889	2.086	1.755
	0		0.450	0.819	0.799

model to the soil, and assign the corresponding constitutive model parameters

(2) The mechanical boundary conditions of the model were set as the left and right boundaries constraining the horizontal displacement, the bottom boundary was set to constrain the horizontal and vertical displacement at the same time, and the upper boundary was free

(3) Set the gravity field and the initial stress ratio to generate the initial stress field

(4) Select single seepage mode. Turn on the fluid mode, assign the fluid isotropy constitutive model, and set the fluid parameters for the constitutive model

(5) Set the fluid boundary conditions and set the front, back, left, right, and bottom as 0 flow boundaries and the top surface as the free surface, which used to simulate to hydrodynamic conditions

(6) Set the calculation yield criterion, obtain the result cloud map, and finally carry out the result analysis

4. Model Test Result Analysis

4.1. The Variation and Dynamic Response of Water-Gas Pressure with Water Level Fluctuation. The constant change of water level in the karst cavity caused by the fluctuation of water level indirectly changes the water-gas pressure in the existing soil cave, thereby affecting the deformation of the soil cave and the overburden [33].

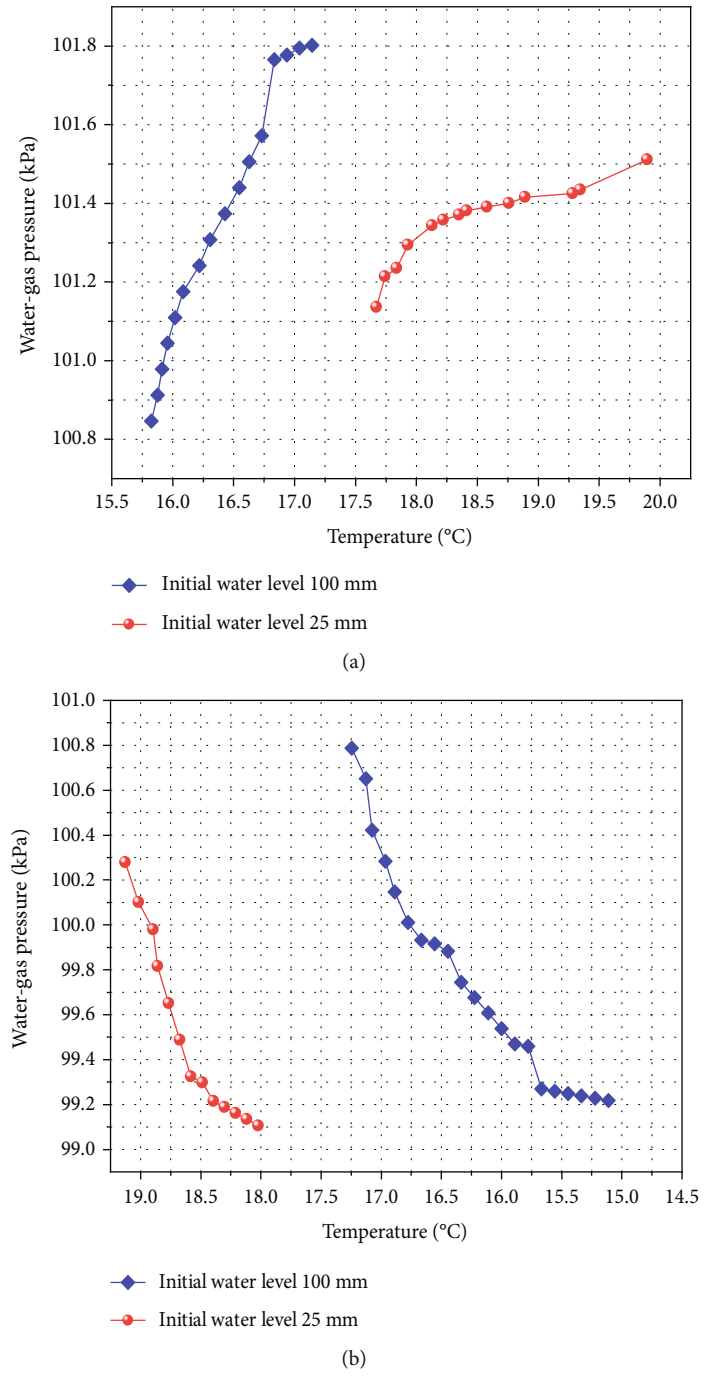

Figure 6: Relationship between water-gas pressure and temperature during water level rise and fall when collapse. (a) Water level rise. (b) Water level drop.

Figure 5 shows the variation of water-gas pressure during the collapse of karst soil caves caused by three groups of different initial water level fluctuations; it is analyzed that the initial water level height has different degrees of influence on the changes of water-gas pressure in the soil and the response of soil deformation:

(1) Under different conditions of initial water level, the change of water-gas pressures in the soil caused by the rise and fall of the water level, and the soil deformation effects are different. The maximum water-gas pressure regions were concentrated at 101.5~102.5 kPa, 101~101.75 kPa, and 99.75~100.25 kPa, and the minimum value areas were concentrated at 98.5~99 kPa, 98.75~99.75 kPa, and 99.13~99.35 kPa, indicating the higher the initial water level, the greater the fluctuation range of the water-air pressure and the stronger the water shock blasting effect on the roof of the existing soil cave during the rise of the water level. Thus, the increase of the water-gas pressure peak was aggravated

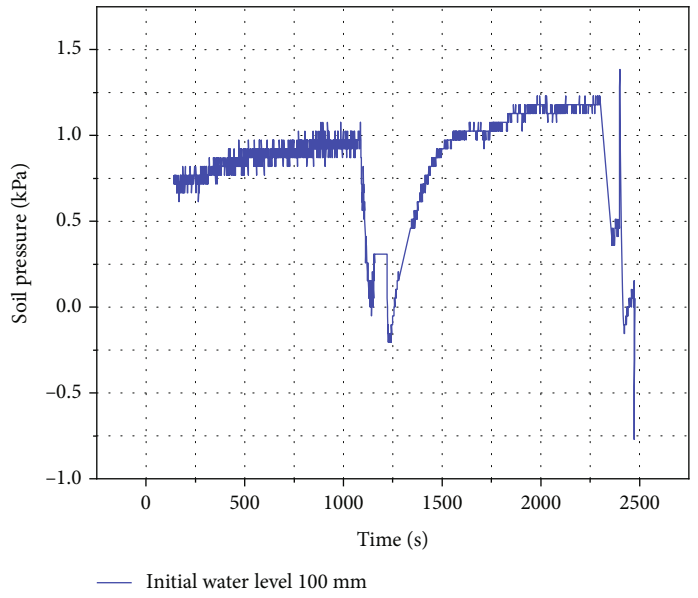

Figure 7: Variation of soil pressure with time.

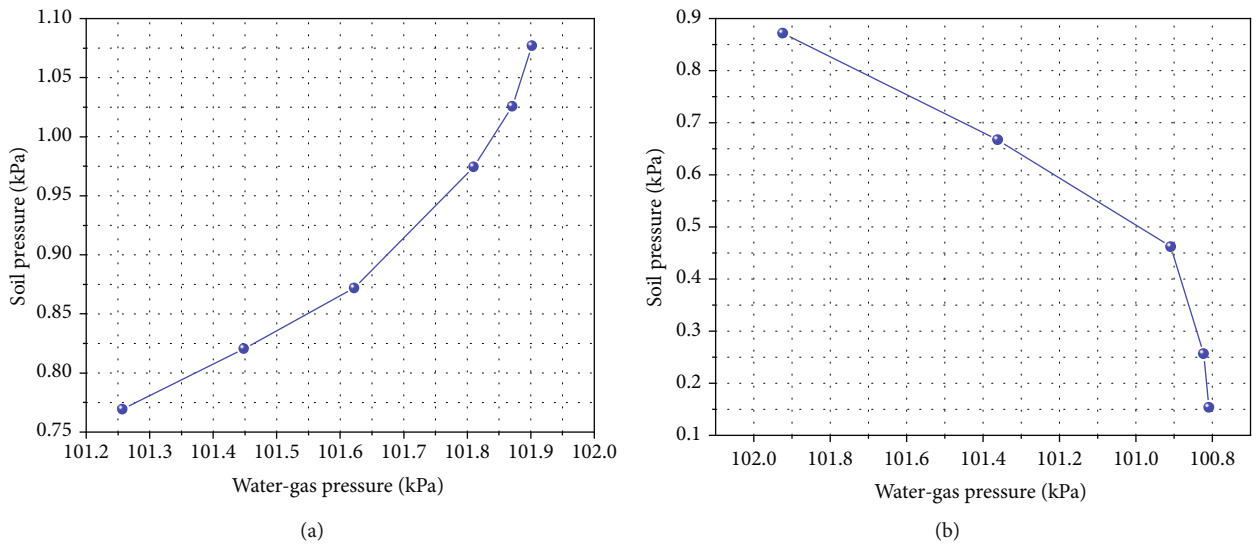

Figure 8: The relationship between soil pressure and water-gas pressure. (a) Water level rise. (b) Water level drop.

due to the compression of the soil cave space, leading to the overlying soil peeling off faster. Correspondingly, when the water level fell, the negative pressure absorption effect on the existing soil cavity was stronger, and the soil exfoliation was accelerated. The soil cavity was partially connected to the atmosphere, and the water-gas pressure dropped rapidly. The fluctuation of the water level caused the overlying soil to slump continuously; when the entire existing soil cave was connected to the atmosphere, the soil cave expanded to the surface of the overlying soil layer to form the collapse

(2) With the rise and fall of the water level, the most prominent feature of the water-gas pressure change in the existing soil cave is sudden and transient. Under the three initial water level conditions, the water-gas pressure changes slowly in the initial stage; as the water level rose in the existing soil cave, it suddenly reached the maximum value, and the minimum value occurred at the moment when the water level drops

(3) The change response of water-gas pressure in the existing soil cave is positively proportional to the initial water level. Under three different initial water levels, the water-gas pressure changed significantly, which lasted for 955 s, 975 s, and 990 s, respectively, and with the increase of the number of water level fluctuations, the response time difference increased gradually

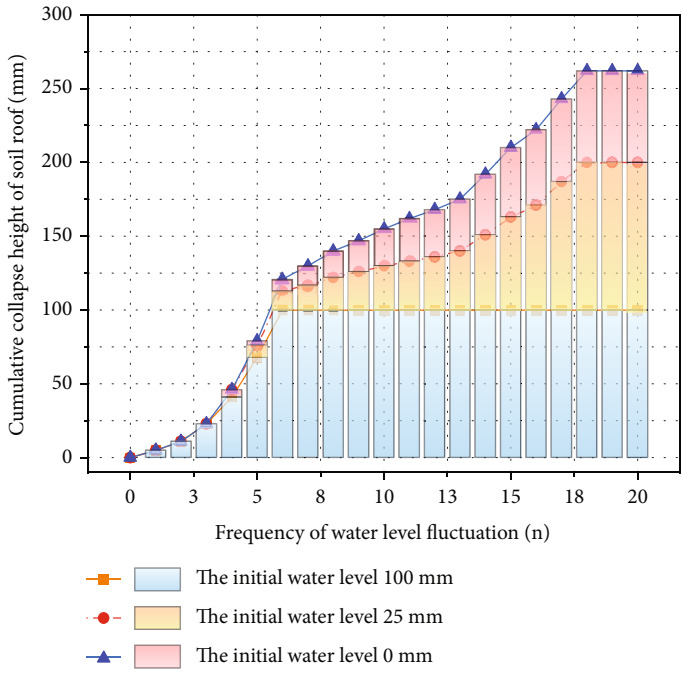

Figure 9: The relationship between the frequency of water level fluctuation and the cumulative slump.

Table 3 shows the increase and decrease of the water-gas pressure with large fluctuations and obvious changes during the rising and falling of different initial water levels. The analysis reveals that in the same process of water level fluctuation, the influence of the water level dropping on soil cave evolution is more significant than that of the water level rising. Compared with the rise of the water level, the water-gas pressure in the existing soil cave responds more quickly to the decline of the water level, and the decline rate is larger, which will accelerate the evolution of the soil cave. When the initial water level height is 100 mm, the dropping of the water level caused the maximum decrease in the water-gas pressure to reach 3.93 kPa; at this time, the negative pressure in the soil cave was the largest, and the overlying soil was subjected to strong negative pressure absorption, which enhanced the impact on the overlying soil of peeling.

Figure 6 explains the relationship between the water-gas pressure and the temperature of the existing soil cave during the rise and fall of the water level when it collapse (when the initial water level is 0 mm, the soil cave does not collapse). The analysis shows that the water-gas pressure positively correlates with the temperature in the existing soil cave. Water-gas pressure will rise and fall with the temperature variation in the soil cave. The temperature variation changes the water-gas pressure, which in turn affects the deformation of the overlying soil: the greater the temperature change, the greater the fluctuation amplitude of the water-gas pressure and the more pronounced the deformation effect on the soil.

4.2. Variation of Soil Pressure in Overburden during Water Level Fluctuation and Its Relationship with Water-Gas Pressure in Soil Cave. Under the condition of three different initial water level heights, the variation law of soil pressure in overburden with time is consistent in the cave-induced karst process caused by water level fluctuation. The condition of the initial water level, which was100 mm, on the surface of the soil layer was taken as an example, and the variation law of the soil pressure and water-gas pressure during the collapse of the karst soil cave was discussed and analyzed based on the experimental data of the laboratory model.

Figure 7 shows the soil pressure change with time during the water level fluctuation. Compared with Figure 5, it can be seen that the water level fluctuation has different effects on the changes of soil pressure in the overburden and water-gas pressure in the soil cave. The increase and decrease of the soil pressure in the overburden are smaller than that of the water-gas pressure in the soil cave because the water-gas pressure in the soil cave does not fully act on the overlying soil. Although the soil and water-gas pressure increase synchronously when the groundwater level rises, the increased speed differs. When the water level rises in the soil cave, the soil pressure and air pressure increase rapidly, and the water pressure increase value is mainly related to the water level height. When the groundwater level drops, the soil and air pressure decrease sharply. The change is associated with the falling speed of the water level, while the change in water pressure is relatively gentle and only relates to the height of the groundwater.

Figure 8 reflects the relationship between the soil pressure and the water-gas pressure during water level rising and falling. The analysis shows that the change of soil pressure in the overburden positively correlates with the shift in water-gas pressure in the soil cave. The water-air pressure generated by the rise of the water level increases the soil pressure of the overlying soil. Correspondingly, the soil pressure decreases when the water level drops, and the reduced amplitude is larger.

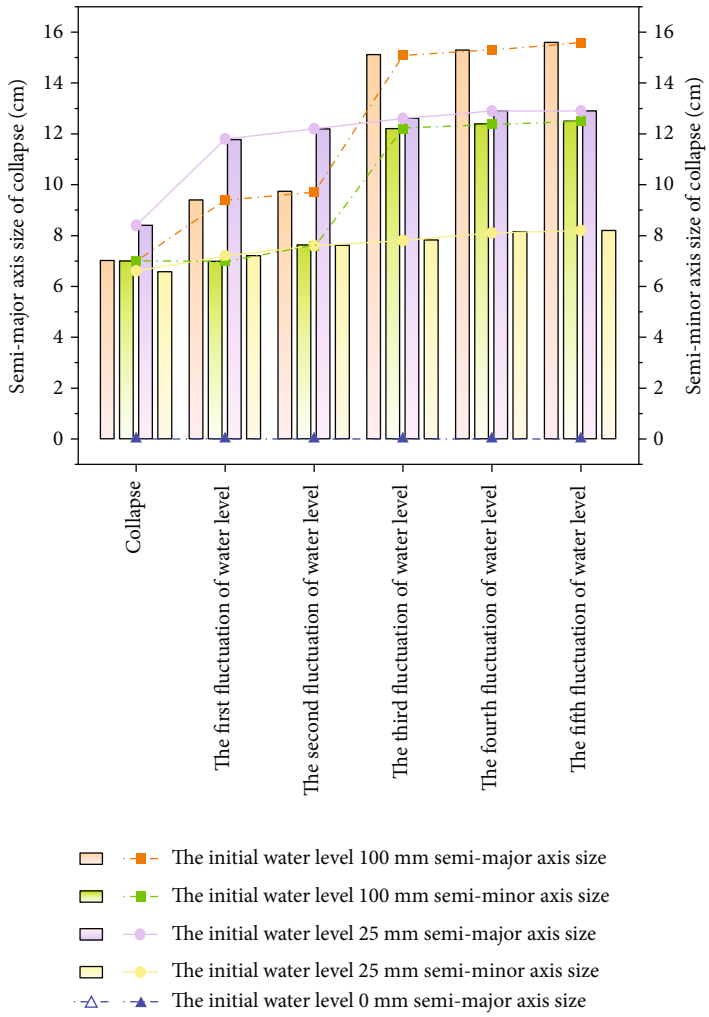

Figure 10: The number of water level fluctuations and the semiaxis length of the collapsed pit.

4.3. Influence of Initial Water Level and Number of Water Level Fluctuations on the Deformation Overlying Soil. Water level fluctuations often cause existing soil caves to collapse. The timeliness and scale of collapse are related to the initial groundwater level and the number of water level fluctuations.

Figure 9 can be analyzed as follows:

(1) The time response of soil exfoliation to the initial water level is different. The time response speed is positively correlated with the initial water level height. The higher the initial water level, the more soil exfoliation can occur when the frequency of water level fluctuation is less, and the faster the slump at the cave's roof is accumulated. When the initial water level height is 100 mm, there are two times water level fluctuations, and local slumps occur in the overlying soil body of the existing soil cave. When the initial water level height is 0 mm, only a tiny amount of soil collapses after five times water level fluctuations. The response time and slump amount are not as good as the higher initial water level

(2) The difficulty of soil cave collapse negatively correlates with the initial water level. When the initial water level height is 100 mm and 25 mm, the soil cave collapses during the water level fluctuation 7 and 18 times, respectively, but it does not collapse when it is 100 mm. The height of the initial water level directly affects the airtightness of the overburden layer and thus changes the hydrodynamic conditions. The higher the initial water level, the stronger the water sealing effect and the better the internal airtightness of the soil body, which enhances the water hammer gas explosion and negative pressure absorption effect on the overlying soil layer. It accelerates the soil exfoliation and makes the soil cave more likely to collapse

(3) The number of water level fluctuations affects the amount of exfoliation of the overlying soil in the existing soil cave. The cumulative amount of slump on the roof of the cave increased most obviously at the moment of collapse. With the increase in the number of water level fluctuations, the cumulative

(a)

(b)

(c)

(d)

Figure 11: Dimensional measurement of collapse opening in model test. (a–d) The measured diagram of the long and short half-axis length during the collapse, one-time water level fluctuation, two times water level fluctuation, and three times water level fluctuation.

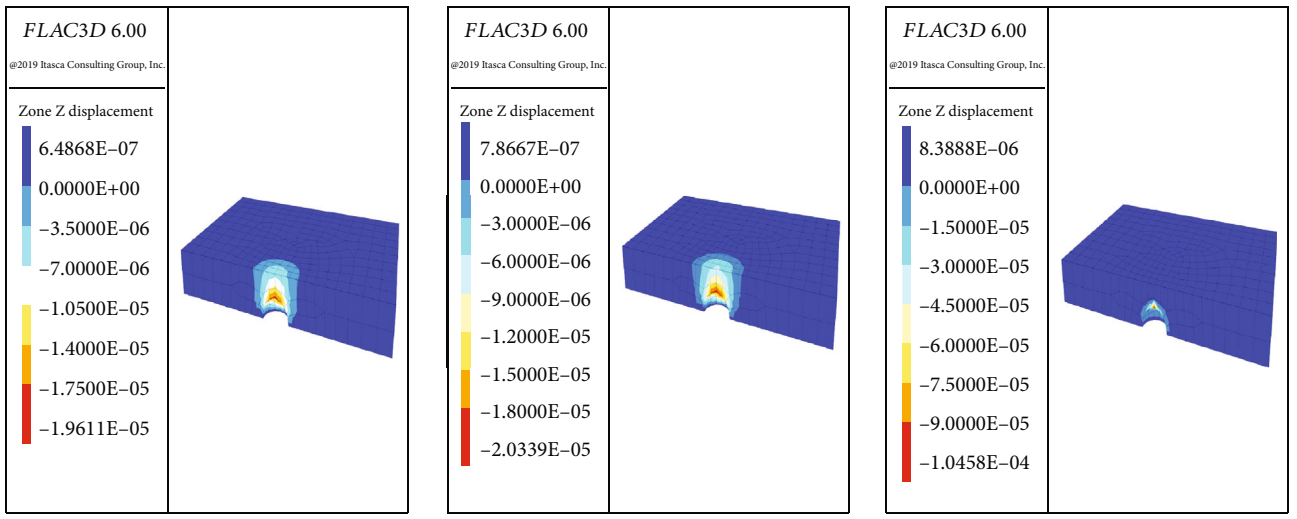

(a)

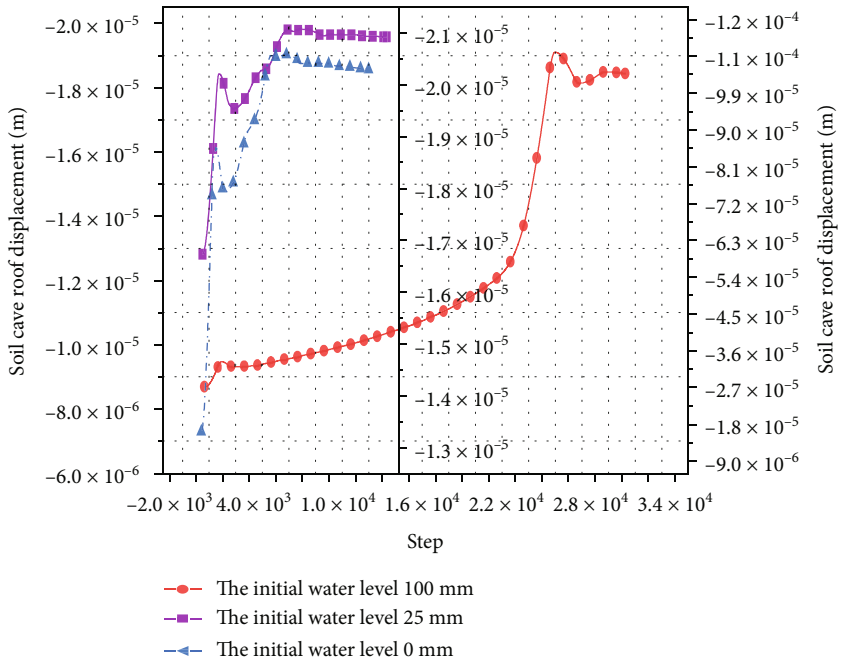

(b)

Figure 12: Continued.

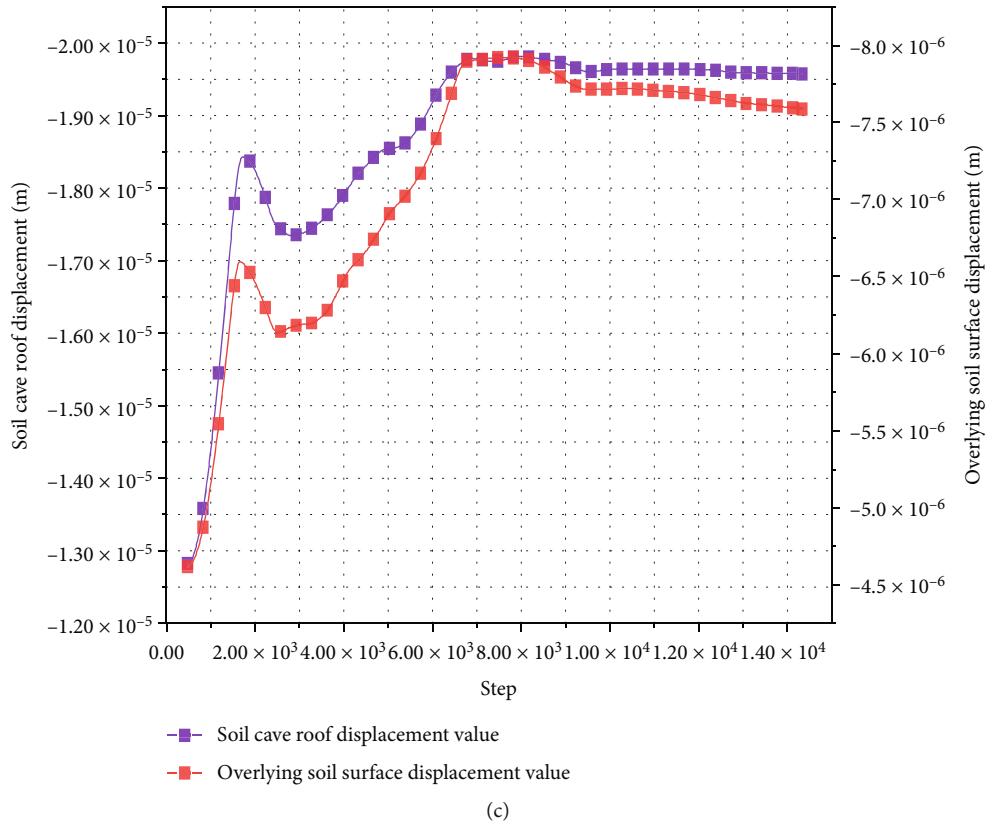

Figure 12: Deformation of overlying soil during water level droping. (a) Variation of cave roof displacement with time steps during the dropping of different initial water levels. (b) Variation of cave roof displacement under different initial water levels dropping. (c) When the initial water level height is 100 mm, the displacement of the roof of cave and the displacement of the overlying soil variation with time steps.

amount of slump continued to increase, but the increased amplitude in the amount of slump decreased accordingly

The length of the collapsed pit and the length of the semiaxis directly reflect the collapse degree of the soil cave. Figure 10 shows the effect of continuous water level fluctuation on the length of the collapsed pit under three different initial water levels after the collapse. It takes the initial water level height at 100 mm as an example and displays the measured size of the change in the semiaxis length of the collapsed pit (Figure 11). As the water level continues to fluctuate, the sidewall and the scale of the collapse pit were mainly subjected to the effects of latent corrosion and continuously peeled off:

(1) The length of the long and short semiaxes of the collapse pit gradually increases with the increase of the number of water level fluctuations and then tends to be stable

(2) The height of the initial water level directly affects the degree of the length of the collapse pit semiaxis change under the water level fluctuations. The higher the initial water level is, the more obvious the change in the semiaxis length of the collapse pit is. When the initial water level height is 100 mm, during the first three water level fluctuations, the change in the semiaxis length of the collapse pit is more obvious than when the initial water level was located in the middle of the soil cave, resulting in the bigger collapse

(3) The initial water level was uncompressed; the water-gas pressure generated by the water level fluctuation was insufficient to cause the karst soil cave to collapse

5. Numerical Simulation Results and Analysis

5.1. Vertical Displacement Results and Analysis. According to the model test results, the water level dropping has a stronger impact on the stability of the soil cave, so the process of the water level dropping under different initial water levels was simulated, and the stress, displacement, and plastic zone development of soil cave and overlying soil were displayed. In the process of water level dropping, the existing soil cave sidewalls and overlying soil were peeled off due to the movement of latent corrosion and negative pressure absorption, the vertical displacement of the roof of the cave was constantly changed, the lateral displacement was carried out along the direction of the toe of the cave, and the scale of the collapse gradually expanded.

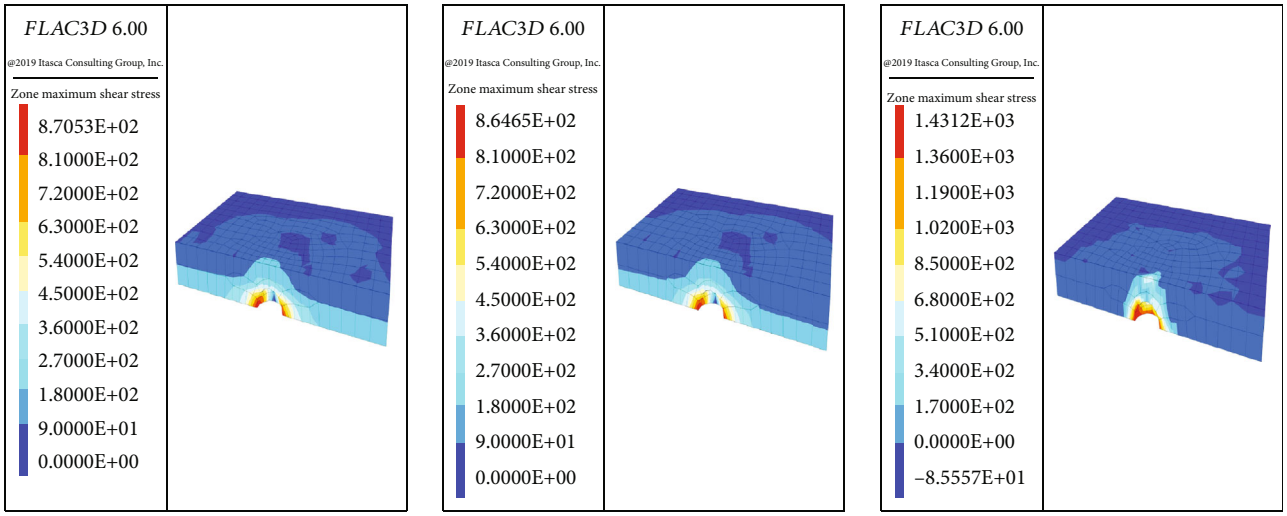

Figure 13: Variation of maximum shear stress during the dropping process with initial water level heights of 0 mm, 25 mm, and 100 mm, respectively.

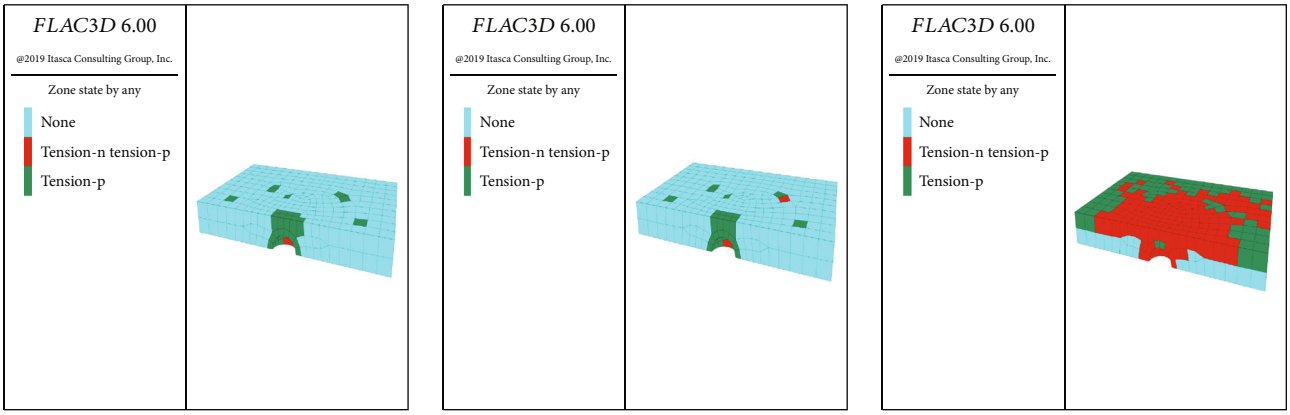

Figure 14: Variation of plastic zone development during the dropping process with initial water level heights of 0 mm, 25 mm, and 100 mm, respectively.

Figure 12(a) shows from left to right the distribution of vertical displacement in the process of water level drop with initial water level heights of 0 mm, 25 mm, and 100 mm, respectively. After analyzing Figures 12(a) and 12(b), it can be seen that the maximum displacement occurred at the roof of the soil cave during the three initial water level dropping processes. The height of the initial water level affects the magnitude of the displacement. The higher the initial water level, the greater the vertical displacement of the roof of the cave. When the initial water level height is 0 mm, this vertical displacement was only 1.96×10^{-5} m; however, when the initial water level height is 100 mm, it reached 1.05×10^{-4} m, an increase of an order of magnitude, mainly due to the high initial water level and the strong airtightness of the soil, increasing the water-gas pressure during the rise of the water level, which has a stronger spalling effect on the soil above the soil cave, and is basically consistent with the physical model test results.

According to Figure 12(c), the analysis shows that in the process of water level dropping, the displacement of the roof of the cave and the displacement of the overlying soil surface was synchronous, and there was a "hysteresis" between them. This is because the slump of the soil cave expanded continuously from bottom to top, and the above soil fell off until it penetrated to the surface, which exists a time effect. Compared with the soil surface displacement, change range, growth rate, and magnitude of the cave roof displacement were higher; this is because the bottom of the cave roof is a free surface, and the soil at the roof of the cave will be directly affected by the combined movement of latent erosion and negative pressure absorption in the process of water level dropping. From the numerical simulation displacement cloud map, the changing law of vertical displacement with water level is basically consistent with the conclusion obtained from the physical model test.

5.2. Shear Stress Results and Analysis. In the process of water level dropping, seepage force and negative pressure absorption force act together on the soil, causing the seepage field and force field to change continuously, and the stress of the entire overlying soil layer is redistributed, and stress concentration occurs at the roof of the cave. When the collapse-inducing force exceeds the shear strength of the entire overlying soil layer, the soil starts to collapse.

As shown in Figure 13, the maximum shear stress presented at the toe of the soil cave in three different initial water level dropping processes. The negative pressure absorption caused by the drop in water level caused the stress redistribution of the overlying soil layer. The stress concentration occurred at the roof of the cave and was transmitted to the toe. When the toe reached the maximum shear stress, the soil began to peel off, and the "soil arch effect" showed at the roof of the cave, resulting in regional damage at the bottom of the soil cave, forming a low value of shear stress area until collapse was formed [34]. The initial water level height is positively proportional to the maximum shear stress change. When the initial water level was on the soil surface, the maximum shear stress was 1.27×10^3 Pa, which accelerated the shear failure of the soil, and the maximum shear stress expanded from the toe to the surrounding soil, which accelerated the collapse. From the cloud map of the numerical simulation of shear stress changes, the stress distribution state and its deformation effect corresponds well to the physical model test phenomena and results.

5.3. Changes and Analysis of Plastic Zone Development. The soil cave is affected by various collapse-inducing forces when the water level drops. When the ultimate shear strength of the soil layer is reached, the soil will enter a state of plastic yield and be destroyed. By simulating the water level dropping under different initial conditions, the development of the plastic zone of the soil cavity was observed, and the stability of the overlying soil layer was judged.

Figure 14 shows that the stability of the soil cave is negatively proportional to the initial water level. The higher the initial water level, the easier the soil cave is to collapse. When the initial water level height is 100 mm, compared with the lower initial water level, the plastic zone of the soil cave develops faster and penetrates to the entire soil surface, resulting in the unstable state of the overlying soil and collapsing occurs. From the cloud map of the numerical simulation of plastic zone development, the plastic zone distribution corresponds well to the physical model test phenomena and results.

6. Conclusion

The collapse of the soil cave results from the joint action of the s effect of latent corrosion, the negative pressure absorption effect, and the positive pressure gas explosion during water level fluctuation. The change of water-gas pressure directly affects the mechanism of soil cave collapse. The height of the initial water level, the soil pressure in the overlying soil layer, and the temperature in the existing soil cave will influence the change of the water-gas pressure to various degrees, thereby affecting the deformation and collapse effect of the soil cave.

(1) The initial water level has a significant impact on the water-gas pressure in the soil cave and the collapse speed of the soil cave. The response of water-gas pressure is positively proportional to the initial water level height, and the response time difference increases gradually with water level fluctuations. The change of water-gas pressure in the existing soil cave and the difficulty degree of soil cave collapse are positively proportional to the initial water level height. The higher the initial water level is, the greater the variation of the water-gas pressure is. The stronger the water shock explosion and negative pressure absorption effect on the existing soil cave, the easier it was to form a collapse

(2) The temperature and the overlying soil pressure are related to the changes in the water-gas pressure in the cave. The water-gas pressure is positively correlated with the temperature in the existing soil cave. The greater the temperature change, the greater the fluctuation amplitude of the water-gas pressure and the more pronounced the deformation effect on the soil. The change of soil pressure in the overlying is positively correlated with the change of water-gas pressure in the soil cave

(3) The number of water level fluctuations has a very obvious influence on the amount of soil exfoliation in the soil cave. With the increase in the number of water level fluctuations, the cumulative amount of slump will continue to increase, but the increased amplitude in the amount of slump will decrease accordingly

(4) The soil cave collapse is caused by comprehensive influencing factors. The height of the initial water level directly affects the degree of the length of the collapse pit and the length of the semiaxis under the frequency of water level fluctuations. Under the same frequency of water level fluctuation, the higher the initial water level, the higher the degree of recollapse

(5) Numerical simulation can better reflect the change of soil cave collapse. The numerical simulation results show that the variation law of stress, displacement, and plastic zone in the soil cave's sidewall and the overlying soil's interior during the water level drop of the three initial water levels are in good agreement with the physical model test results

(6) The paper has some limitations in applying similarity theory, experimental operation, and the simulation of hydrodynamic conditions. The simulation of the soil layer in the physical model only considers the geometric similarity ratio; the boundary conditions' setting cannot fully reflect the complex boundary conditions of the study area. Humans control the water level fluctuation conditions so that the water level flow direction cannot entirely reflect the actual flow state of the groundwater level, which requires further improvement and research

Data Availability

The data used to support the findings of this study are included in the article.

Conflicts of Interest

The authors declare that they have no conflicts of interest.

Acknowledgments

This work was initiated with support from the National Natural Science Foundation of China NSFC Grant (No. 41967037) and was continued with support from the National Key Research and Development Program Grant (No. 2019YFC507502).

References

[1] Y. B. He and C. Xu, "On the hydrodynamics of karst collapse," *Hydrogeology and Engineering Geology*, vol. 5, pp. 39–42, 1993.

[2] X. A. Li, R. Q. Huang, J. B. Peng, and Z. Chen, "Establishent of conceptual models of physical sub-ground erosion," *Journal of Engineering Geology*, vol. 18, no. 6, pp. 880–886, 2010.

[3] X. J. Luo and C. Luo, "Three-mechanism theory (TMT) of karst ground collapse and its application," *Carsologica Sinica*, vol. 40, no. 2, pp. 171–188, 2021.

[4] Y. Y. Wei and S. L. Sun, "Study on formation and expansion condition of hidden soil cavity under condition of groundwater exploitation in karst areas," *Environmental Earth Sciences*, vol. 76, no. 7, p. 282, 2017.

[5] K. Q. He, B. Wang, and D. Y. Zhou, "Mechanism and mechanical model of karst collapse in an over-pumping area," *Environmental Geology*, vol. 46, no. 8, pp. 1102–1107, 2004.

[6] B. Wang and K. Q. He, "Study on limit equilibrium height expression of critical soil cave of karst collapse," *Rock and Soil Mechanics*, vol. 27, no. 3, pp. 458–462, 2006.

[7] X. Chen, R. Guo, L. Tang, and X. Zhang, "Study on ground collapse of covered karst soil caves by sudden drop of groundwater," *Advances in Civil Engineering*, vol. 2021, Article ID 7796401, 12 pages, 2021.

[8] R. J. Guo, X. J. Chen, J. Duan, T. Lingming, and Z. Xiaochen, *Study on precipitation-induced subsidence of covered karst soil cave considering spatial shape*, Journal of Southwest Jiaotong University, 2022, http://cnki.net/kcms/detail/51.1277.U.20220712.1148.006.html.

[9] Y. Xue, P. G. Ranjith, Y. Chen, C. Cai, F. Gao, and X. Liu, "Nonlinear mechanical characteristics and damage constitutive model of coal under CO_2 adsorption during geological sequestration," *Fuel*, vol. 331, no. 1, article 125690, 2023.

[10] Z. B. Lin, B. Y. Zhang, and J. Q. Guo, "Analysis of a water-inrush disaster caused by coal seam subsidence karst collapse column under the action of multi-field coupling in taoyuan coal mine," *Computer Modeling in Engineering Sciences*, vol. 126, no. 1, pp. 311–330, 2021.

[11] X. J. Chen, M. F. Zhou, F. J. Chen, and M. G. Xiao, "Destructive pumping test to study the characteristics of karst collapse in limestone region: a case study in the western urban area of Guilin city," *Geological Science and Technology Information*, vol. 21, no. 1, pp. 79–82, 2001.

[12] X. Z. Jiang, M. T. Lei, and Y. L. Gao, "Formation mechanism of large sinkhole collapses in Laibin, Guangxi, China," *Environment and Earth Science*, vol. 76, no. 24, pp. 810–823, 2017.

[13] L. Jia, L. J. Li, Y. Meng, Y. Wu, Z. Pan, and R. Yin, "Responses of cover-collapse sinkholes to groundwater changes: a case study of early warning of soil cave and sinkhole activity on Datansha Island in Guangzhou, China," *Environmental Earth Sciences*, vol. 77, no. 13, pp. 1–11, 2018.

[14] M. T. Lei, X. Z. Jiang, and Y. Li, "Karst collapse model test-taking Wuchang as an example," *Geological Hazards and Environmental Preservation*, vol. 4, no. 2, pp. 39–44, 1993.

[15] F. W. Jiang, "Simulation experiment on sinkhole formation caused by soils disintegration and the advance-forecasting of sinkhole risk," *Environmental Earth Sciences*, vol. 79, no. 19, pp. 1–9, 2020.

[16] H. Shi, Q. M. Li, Q. L. Zhang, Y. Yu, Y. Xing, and K. Yu, "Mechanism of shallow soil cave–type karst collapse induced by water inrush in underground engineering construction," *Journal of Performance of Constructed Facilities*, vol. 34, no. 1, pp. 1–8, 2020.

[17] J. Shen, W. B. Jian, T. J. Su, R. B. Bao, and S. B. Zhang, "Study on the evolution process of soil cave collapse in karst area-taking the soil cave collapse in Zhangkeng natural village, Longyan City as an example," *Journal of Water Conservancy and Construction Engineering*, vol. 18, no. 3, pp. 1–8, 2020.

[18] Q. H. Wu, W. Zhang, Y. Liu, and H. D. Cui, "Quantifying the process of karst collapse by a physical model," *Journal of Yangtze River Scientific Research Institute*, vol. 35, no. 3, pp. 52–58, 2018.

[19] W. M. Yang, X. Yang, Z. D. Fang et al., "Model test for water inrush caused by karst caves filled with confined water in tunnels," *Arabian Journal of Geosciences*, vol. 12, no. 24, pp. 1–11, 2019.

[20] D. Ma, H. Y. Duan, X. B. Li, Z. Li, Z. Zhou, and T. Li, "Effects of seepage-induced erosion on nonlinear hydraulic properties of broken red sandstones," *Tunnelling and Underground Space Technology*, vol. 91, article 102993, 2019.

[21] X. X. Xiao, Z. F. Li, G. Q. Cai, and H. Yang, "Effects of declining water levels on water-air interactions in cover collapse sinkhole," *Bulletin of Engineering Geology and the Environment*, vol. 80, no. 3, pp. 2545–2556, 2021.

[22] X. X. Xiao, F. Gutiérrez, and J. Guerrero, "The impact of groundwater drawdown and vacuum pressure on sinkhole development. Physical aboratory models," *Engineering Geology*, vol. 279, article 105894, 2020.

[23] S. Zhang, W. Jian, R. Hong, P. Huang, H. Chen, and B. Liu, "Experimental study on collapse of covered karst under water-level fluctuation," *Journal of Engineering Geology*, vol. 27, no. 3, pp. 659–667, 2019.

[24] R. B. Hong, W. B. Jian, and X. Z. Chen, "Study on the response of covered karst soil cave to groundwater fluctuation and its collapse evolution process," *Journal of Engineering Geology*, vol. 2020, pp. 1–9, 2022.

[25] H. Lin, T. Y. Liu, J. T. Li, and P. Cao, "A simple generation technique of complex geotechnical computational model," *Mathematical Problems in Engineering*, vol. 2013, Article ID 863104, 8 pages, 2013.

[26] H. L. Liu, L. C. Li, Z. C. Li, and G. Yu, "Numerical modelling of mining-induced inrushes from subjacent water conducting karst collapse columns in northern China," *Mine Water and the Environment*, vol. 37, no. 4, pp. 652–662, 2018.

[27] S. Lee, J. Y. Park, J. H. Kihm, and J. M. Kim, "Geomechanical and hydrogeological validation of hydro-mechanical two-way sequential coupling in TOUGH2-FLAC3D linking algorithm with insights into the Mandel, Noordbergum, and Rhade effects," *Geomechanics and Engineering*, vol. 28, no. 5, pp. 437–454, 2022.

[28] L. W. Guo, S. L. Wang, L. M. Sun, Z. Kang, and C. Zhao, "Numerical simulation and experimental studies of karst caves collapse mechanism in fractured-vuggy reservoirs," *Geofluids*, vol. 2020, Article ID 8817104, 21 pages, 2020.

[29] Q. H. Xiong, X. Gao, Q. Xu, R. Q. Wang, Z. C. Li, and L. Tao, "Study on numerical model of dynamic evolution of overburden karst collapse," *Safety and Environmental Engineering*, vol. 29, no. 1, pp. 85–92, 2022.

[30] Z. Zhou, Y. L. Xu, C. Q. Zhu, M. T. Xu, and Z. Y. Jin, "Collapse mechanism of shallow-buried karst cave under the effect of mining," *Geotechnical and Geological Engineering*, vol. 39, no. 2, pp. 1521–1532, 2021.

[31] L. Jia, Y. Meng, L. J. Li, and R. Yin, "A multidisciplinary approach in cover-collapse sinkhole analyses in the mantle karst from Guangzhou City (SE China)," *Natural Hazards*, vol. 108, no. 1, pp. 1389–1410, 2021.

[32] E. Fumagalli, "Model simulation of rock mechanics problem," in *Rock Mechanics in Engineering Practice*, vol. 38, J. Wiley Bulletin Ismes Nr, London, 1968.

[33] D. Ma, X. X. Miao, H. B. Bai et al., "Effect of mining on shear sidewall groundwater inrush hazard caused by seepage instability of the penetrated karst collapse pillar," *Natural Hazards*, vol. 82, no. 1, pp. 73–93, 2016.

[34] L. Jia, Y. Meng, Z. D. Guan et al., "Evolution and numerical simulation of a karst soil cave," *Carsologica Sinica*, vol. 33, no. 3, pp. 294–298, 2014.